

Three-Dimensional Structure of the Wind-Driven Circulation in the Subtropical North Pacific*

RUI XIN HUANG

Department of Physical Oceanography, Woods Hole Oceanographic Institution, Woods Hole, Massachusetts

BO QIU

Department of Oceanography, SOEST, University of Hawaii, Honolulu, Hawaii

(Manuscript received 5 August 1993, in final form 16 December 1993)

ABSTRACT

The subduction rate is calculated for the North Pacific based on Levitus climatology data and Hellerman and Rosenstein wind stress data. Because the period of effective subduction is rather short, subduction rates calculated in Eulerian and Lagrangian coordinates are very close. The subduction rate defined in the Lagrangian sense consists of two parts. The first part is due to the vertical pumping along the one-year trajectory, and the second part is due to the difference in the winter mixed layer depth over the one-year trajectory. Since the mixed layer is relatively shallow in the North Pacific, the vertical pumping term is very close to the Ekman pumping, while the sloping mixed layer base enhances subduction, especially near the Kuroshio Extension. For most of the subtropical North Pacific, the subduction rate is no more than 75 m yr^{-1} , slightly larger than the Ekman pumping. The water mass volume and total amount of ventilation integrated for each interval of 0.2σ unit is computed. The corresponding renewal time for each water mass is obtained. The inferred renewal time is 5–6 years for the shallow water masses ($\sigma = 23.0\text{--}25.0$), and about 10 years for the subtropical mode water ($\sigma = 25.2\text{--}25.4$).

Within the subtropical gyre the total amount of Ekman pumping is 28.8 Sv ($\text{Sv} = 10^6 \text{ m}^3 \text{ s}^{-1}$) and the total subduction rate is 33.1 Sv, which is slightly larger than the Ekman pumping rate. To this 33.1 Sv, the vertical pumping contributes 24.1 Sv and the lateral induction 9 Sv. The maximum barotropic mass flux of the subtropical gyre is about 46 Sv (east of 135°E). This mass flux is partitioned as follows. The total horizontal mass flux in the ventilated thermocline, the seasonal thermocline, and the Ekman layer is about 30 Sv, and the remaining 16 Sv is in the unventilated thermocline. Thus, about one-third of the mass flux in the wind-driven gyre is sheltered from direct air–sea interaction.

1. Introduction

Motion in the upper one kilometer of the ocean is primarily wind driven. The horizontal and vertical motion in this layer control the interaction between the atmosphere and the oceans. Thus, the structure of the wind-driven circulation is of vital importance for our understanding of oceanic general circulation and climate. In the early stages of developing the wind-driven circulation theory, our understanding was primarily two-dimensional in nature. For example, the most frequently cited indices for the wind-driven circulation are the total amount of Ekman flux across a latitude circle, the total amount of Ekman pumping,

and the maximum barotropic mass fluxes of the subtropical/subpolar gyres. Although these indices give useful information about the wind-driven circulation, they convey little about atmosphere–ocean interaction. For example, these indices do not show how deep the wind-driven circulation can penetrate nor how fast the climate anomalies at the sea surface can propagate into subsurface layers. To answer these questions, one needs to unravel the vertical structure of the wind-driven circulation.

Before the 1980s, theories about the vertical structure of the wind-driven circulation were mostly similarity solutions. These theories treat the entire water column of the wind-driven circulation indiscriminately. In the 1980s, theories about the baroclinic structure of the wind-driven gyre advanced rapidly. The major difference from the old theories is the recognition of different dynamic zones in the wind-driven circulation. According to the new theories, the thermocline can be separated into the ventilated and unventilated regions. The upper part of the thermocline is directly exposed to the air–sea interaction through mass exchange with

* Woods Hole Oceanographic Institution Contribution Number 8443.

Corresponding author address: Dr. Rui Xin Huang, Department of Physical Oceanography, Woods Hole Oceanographic Institution, Woods Hole, MA 02543.

the mixed layer, thus it is called the ventilated thermocline. The lower part of the thermocline is isolated from direct air-sea interaction, so it is called the unventilated thermocline.

In a series of papers, Rhines and Young (1982a,b) proposed the potential vorticity homogenization theory and applied it to the deep part of the wind-driven circulation, the unventilated thermocline. According to their theory, in the inviscid limit potential vorticity is homogenized for most of the unventilated thermocline due to repeated motions along closed geostrophic contours. Another major breakthrough was the multilayer model for the ventilated thermocline by Luyten et al. (1983). According to their theory, water is subducted from the mixed layer into the upper part of the thermocline, in which water particles continue their journey, preserving the potential vorticity forged during the subduction process.

A major conceptual difficulty associated with the subduction process was the complicated seasonal cycle in the upper ocean. Stommel (1979) presented a simple and elegant view of the subduction process, which is now called the "Stommel demon." Basically, the mixed layer density and depth reach their local maxima at late winter; since the mixed layer rapidly retreats in early spring, water subducted into the permanent thermocline is strongly biased toward the late winter value. Although Iselin (1939) had found the connection between the winter conditions at the sea surface and the water mass characters in the permanent thermocline below, there was no simple dynamic theory to explain their connection. The Stommel demon and the Luyten-Pedlosky-Stommel model have provided a solid dynamic framework for interpreting the water mass formation processes in the upper ocean.

For simplicity, the mixed layer was neglected in the original multilayer model of the ventilated thermocline. The dynamic role of the mixed layer in the ventilation/subduction process was emphasized by Woods (1985). Most importantly, the horizontal gradient of mixed layer depth can substantially enhance the subduction rate. The enhancement of the subduction rate over the Ekman pumping has been demonstrated by Sarmiento (1983) and Jenkins (1982, 1987) through tracer distributions within the thermocline.

Theories for the ventilated and unventilated thermocline were extended to form a unified theory for the three-dimensional structure of a continuously stratified ocean (Huang 1990). In the unified theory the early work about ideal fluid thermocline by Welander (1959) and Needler (1971) is combined with the new developments made by Rhines and Young (1982a,b) and Luyten et al. (1983). Although the theory provides much physical insight into the wind-driven circulation in the upper ocean, the current theory of the ideal-fluid thermocline primarily treats the thermocline as a perturbation to a basic state that is set up by the thermohaline process not explicitly sim-

ulated in the model. Furthermore, most of the new theories can only apply to the time-independent problem. In addition, the thermodynamic properties of the mixed layer, such as the density and depth, are specified as input data. For a comprehensive review of the progress on the structure of wind-driven circulation, the reader is referred to Huang (1991). Although theories about the vertical structure of the wind-driven circulation have been developed, their application to the world oceans has been slow at best. It is only very recently that the vertical structure of the wind-driven circulation in the North Atlantic has been analyzed in light of the new theories (Huang 1990; Marshall et al. 1993; Williams et al. 1994).

It is well known that the general circulation in the North Pacific is quite different from that in the North Atlantic. For example, the thermohaline circulation in the North Pacific is controlled by excess precipitation. As a result, the mixed layer is relatively shallow. In addition, the zero-Ekman-pumping line is very close to a latitude circle. Thus, one expects that the vertical structure of the wind-driven circulation in the North Pacific is different from that in the North Atlantic.

Although the barotropic structure of the subtropical gyre is easily obtained from a simple integration of the wind stress curl, it is not clear how this mass flux is partitioned among the isopycnals. Because the Pacific covers a major part of the earth's surface, clarifying the baroclinic structure of the wind-driven circulation is crucial to our understanding of global air-sea interaction. Thus, our goal is to examine the vertical structure of the subtropical North Pacific, especially the mass exchange rate between the mixed layer and the permanent thermocline. This study is organized as follows. The subduction rate is defined in section 2, where a Lagrangian mean subduction rate is defined. The structure of the wind-driven gyre in the subtropical Pacific is analyzed based on the Levitus (1982) climatology data and the Hellerman and Rosenstein (1983, hereafter HR) wind stress data. Based on the subduction rate and water mass volume, the renewal time of subtropical water masses is calculated in section 3. Finally, we conclude in section 4.

2. The subduction rate

A key element in exploring the vertical structure of the wind-driven circulation is the calculation of the subduction rate. As pointed out by Stommel (1979), although subduction happens most times of the year, water subducted into the permanent thermocline is strongly biased toward late winter properties. Such a strong bias is due to the rapid shoaling of the mixed layer in early spring; thus, the subducted water has the properties typical of late winter, such as the temperature and salinity. In addition, the potential vorticity of the subducted water acquires the potential vorticity setup at late winter by the combination of the mixed-layer

boundary conditions and the large-scale geostrophic flow beneath the mixed layer. As shown by Marshall et al. (1993) and Williams et al. (1994), the subduction period diagnosed from climatology or from numerical results of a primitive equation model is rather short (about 1–2 months) for most of the subtropical basin. Therefore, the subduction rate calculated based on the Stommel demon is accurate enough as a practical way of calculation. As shown in the Appendix, the subduction rate calculated by the Eulerian and Lagrangian coordinates gives similar results for general cases. Thus, we use the Lagrangian definition following Woods and Barkmann (1986).

The Lagrangian subduction rate is defined as

$$S_{\text{ann}} = -\int_0^1 w_{\text{tr}} dt - \int_0^1 \mathbf{v} \cdot \nabla h_m dt, \quad (1)$$

where the integration is taken along the trajectory starting from March of the first year and ending in March of the second year, w_{tr} is the vertical velocity along the water parcel trajectory, h_m is the depth of the mixed layer. The trajectories are determined by integrating the three-dimensional velocity of water parcels released from the base of the mixed layer in March. The first term represents the contribution from the vertical pumping at the base of the mixed layer, and the second term represents the contribution from the lateral induction (due to the slope of the mixed layer base). The above definition can be rewritten as

$$S_{\text{ann}} = (d_2 - d_1) + (h_{m,1} - h_{m,2}), \quad (2)$$

where d_1 and d_2 are the depths of the trajectory in the first and second March, and $h_{m,1}$ and $h_{m,2}$ are the mixed layer depths in the first and second March along the trajectory. However, downward heat flux in the upper ocean reduces the density along the trajectory, so the depth change along the trajectory tends to overestimate the contribution due to vertical pumping. Our calculation indicates that in the middle of the subtropical gyre, the $(d_2 - d_1)$ term can reach to 100 m/yr, which is much larger than the maximum Ekman pumping velocity of 60 m/yr. Thus, the error involved in this approach is too large, and we have chosen the following definition:

$$S_{\text{ann}} = -\left(w_{\text{Ek}} - \frac{\beta}{f} \int_{-d}^0 v dz \right) + (h_{m,1} - h_{m,2}), \quad (3)$$

where w_{Ek} is the Ekman pumping velocity calculated from the Hellerman and Rosenstein (1983) wind stress data, and the β term is a correction due to the meridional velocity in the surface layer; the overbar indicates an averaging over a one-year Lagrangian trajectory. Note that (3) is equivalent to (2) for an ideal-fluid ocean; however, they differ for the real oceans due to mixing/diffusion. Equation (3) may not be very accurate within the recirculation gyre because the inertial

terms are important in this region, so the linear vorticity equation is no longer valid.

Notice that our definition of annual mean subduction rate is strictly a Lagrangian mean averaged over a one-year trajectory similar to that used by Woods and Barkmann, but slightly different from that used by Marshall et al. (1993). In this definition the subduction rate depends not only on the local properties, but also on the alongtrajectory properties.

In our calculation the annual mean subduction rate S_{ann} is computed from (3) over the North Pacific subtropical gyre as follows:

1) The March mixed layer density and mixed layer depth are based on the Levitus climatology (Fig. 1), where the mixed layer density is calculated using the March temperature and winter salinity data, and the mixed layer depth is defined as the depth at which σ_θ differs by 0.125 from the surface σ_θ . The mixed layer density distribution is mostly zonal, except in the eastern part of the subpolar basin where the excess precipitation creates a shallow halocline; thus, the low salinity water is relatively light and gives rise to a northeastern orientation of isopycnals. In most of the North Atlantic, evaporation dominates so isopycnals have a southeastern orientation in the eastern basin. In the subpolar basin where precipitation is somewhat stronger than evaporation, however, isopycnals tilt slightly in the northeastern direction.

The winter mixed layer depth (Fig. 1b) shows a general poleward deepening. There is also a very strong east–west asymmetry. In the southeast corner of the basin the mixed layer depth is about 25 m. It is more than 175 m in the northwest corner of the basin, where the surface heat flux from the ocean to the atmosphere reaches 200–300 W m⁻² because very cold polar air from the continent blows over the ocean in the winter season. The mixed layer depth increases downstream of the Kuroshio and south of the Kuroshio Extension. The increase in the mixed layer depth downstream of the Kuroshio is limited because the thermocline is shallow and convection cannot penetrate deeply. South of the Kuroshio Extension, however, the thermocline is deep, so convection can penetrate to a greater depth. As a result, the largest mixed layer depth is closely tied to the recirculation zone south of the Kuroshio (Bingham 1992).

In general, the mixed layer depth in the North Pacific is substantially shallower than that in the North Atlantic. The difference in mixed layer depth reflects the subtle difference in the thermohaline circulation in these two basins. Since in the North Pacific precipitation exceeds evaporation, a halocline develops in the upper ocean that confines the winter convection to a relatively shallow layer. The low salinity also contributes to the less dense water masses formed in the North Pacific, as seen from the winter mixed layer density map (Fig. 1a).

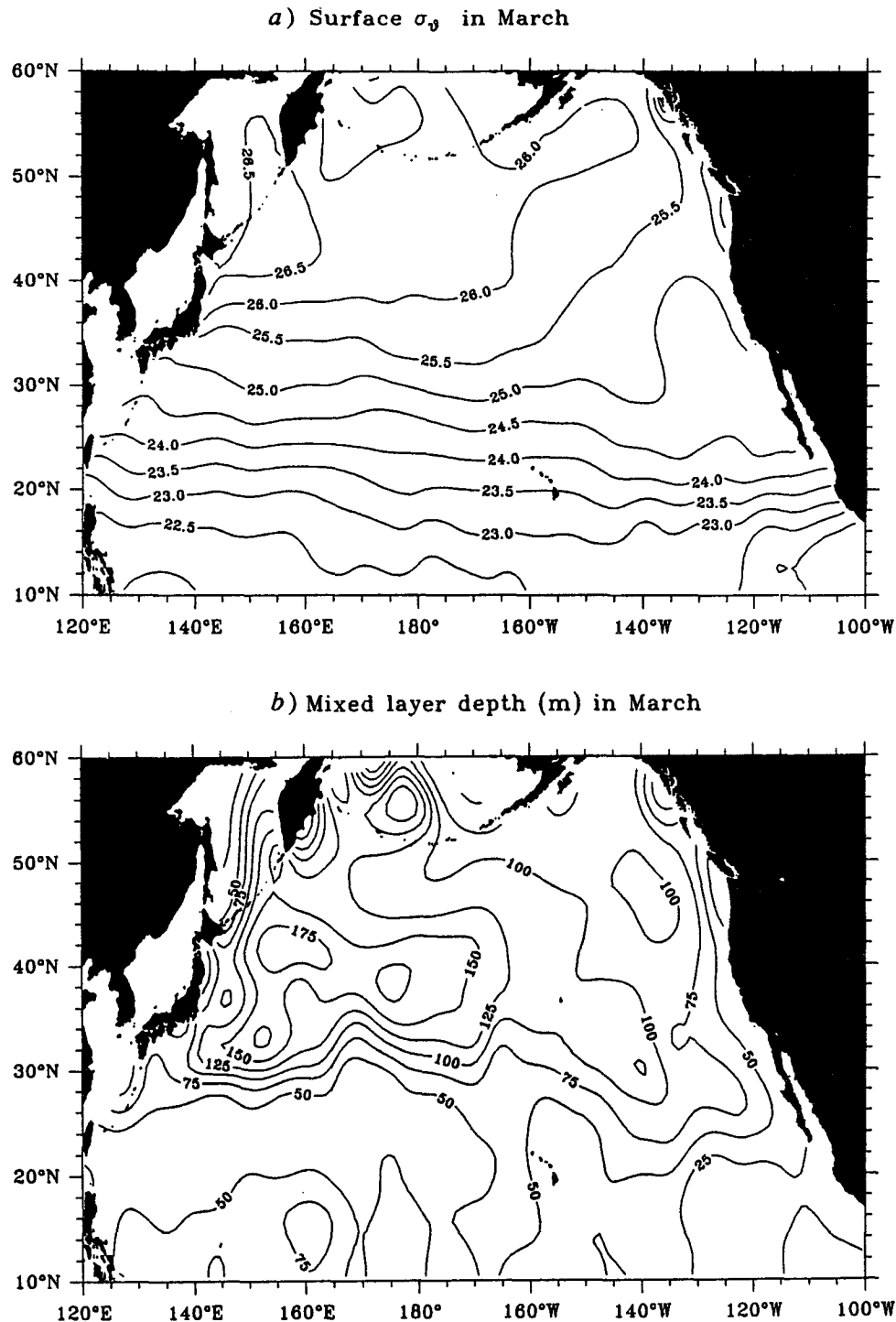


FIG. 1. Winter (March) mixed layer density (a) and depth (b), using Levitus (1982) climatology.

We have followed Levitus (1982) by defining the base of the mixed layer as the depth where the local density is $\Delta\sigma_\theta = 0.125$ heavier than that on the sea surface. Since density stratification in the oceans is

continuous, the depth of the mixed layer is not uniquely defined. We have used a slightly different definition, in which the depth of the mixed layer is defined as the depth where the density increases to $\Delta\sigma_\theta = 0.085$; the

Lagrangian trajectories for a year

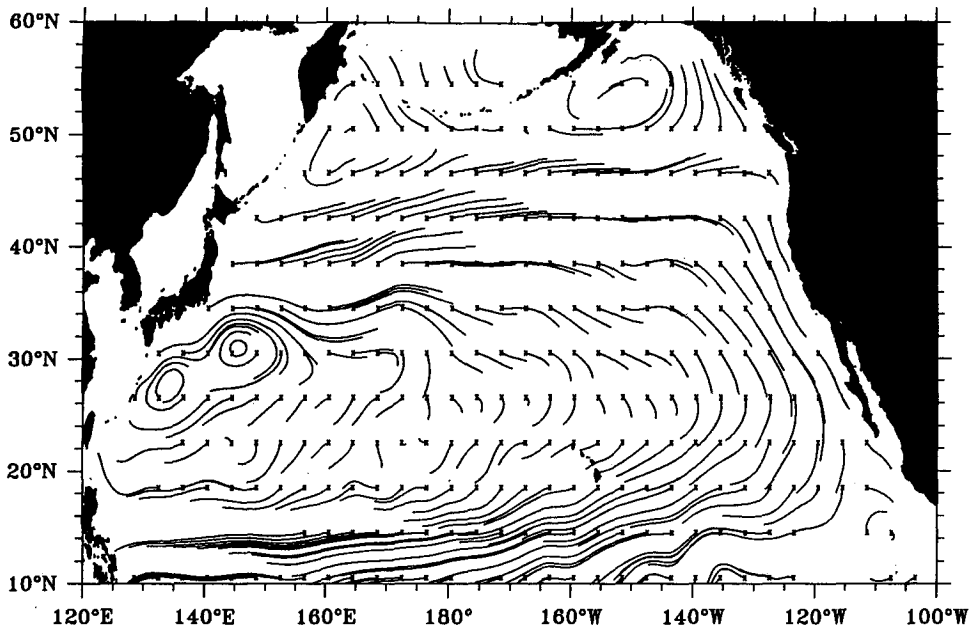


FIG. 2. Lagrangian trajectories over a one-year period. The starting points are indicated by crosses where the particles are released from the base of the mixed layer in March.

map of the mixed layer depth looks very similar to the one used in our calculation, except it shoals by about 30 m. This is relatively small compared with the maximum depth of 175 m. Differences in data and methods of processing the data may give rise to different subsidence rates; however, since our focus is on the gross structure of the subsidence/ventilation, such difference is left for further study.

2) The annual mean horizontal velocity is calculated from the annual Levitus (1982) climatology by integrating the thermal wind equations from a reference level of 2000 m. This level was shown by Roemmich and McCallister (1989) to be appropriate for the subtropical and subpolar North Pacific. To obtain the horizontal velocity on a given isopycnal surface, the acceleration potential A is calculated by integrating the density anomaly from the reference level. The acceleration potential A is defined according to Montgomery and Stroup (1962) as

$$A = \phi_a + p\delta = p_0\delta_0 + \int_{\delta_0}^{\delta} p d\delta,$$

where

$$\phi_a = \int_p^{p_0} \delta dp$$

is the geopotential, p_0 is the reference pressure, δ is the specific volume anomaly, and δ_0 is the specific volume anomaly at the reference pressure. From the equation

above, the definition of geopotential is obtained by changing the variable of integration.

After the acceleration potential is calculated, the geostrophic velocity can be calculated by using

$$-2\Omega \sin\phi v = -\frac{1}{a \cos\phi} \frac{\partial A}{\partial \lambda} \quad (4)$$

$$2\Omega \cos\phi u = -\frac{1}{a} \frac{\partial A}{\partial \phi}, \quad (5)$$

where a is the radius of the earth, ϕ is latitude, λ is longitude, and Ω is the rotation rate of the earth. The horizontal trajectory of a water parcel released from the base of the winter mixed layer can be calculated accordingly. Figure 2 shows some typical Lagrangian trajectories started from different locations in the ocean. Figure 3 shows the contour maps of the acceleration potential and the depth of the two isopycnal surfaces $\sigma_\theta = 25.0$ and 26.2 .

The geostrophic contours on $\sigma_\theta = 25.0$ and 26.2 reveal the general shape of the anticyclonic gyre in the subtropical basin, including the recirculation south of the Kuroshio Extension near 30°N , 145°E (Fig. 3). In fact, the recirculation appears as two cells separated by the Izu Ridge. Notice that the recirculation appears in the form of a C-shape feature in a high-resolution map (Tsuchiya 1982). Furthermore, the recirculation cells have a strong barotropic structure as the centers of these cells are vertically aligned. In the subtropical interior, the central latitude of the

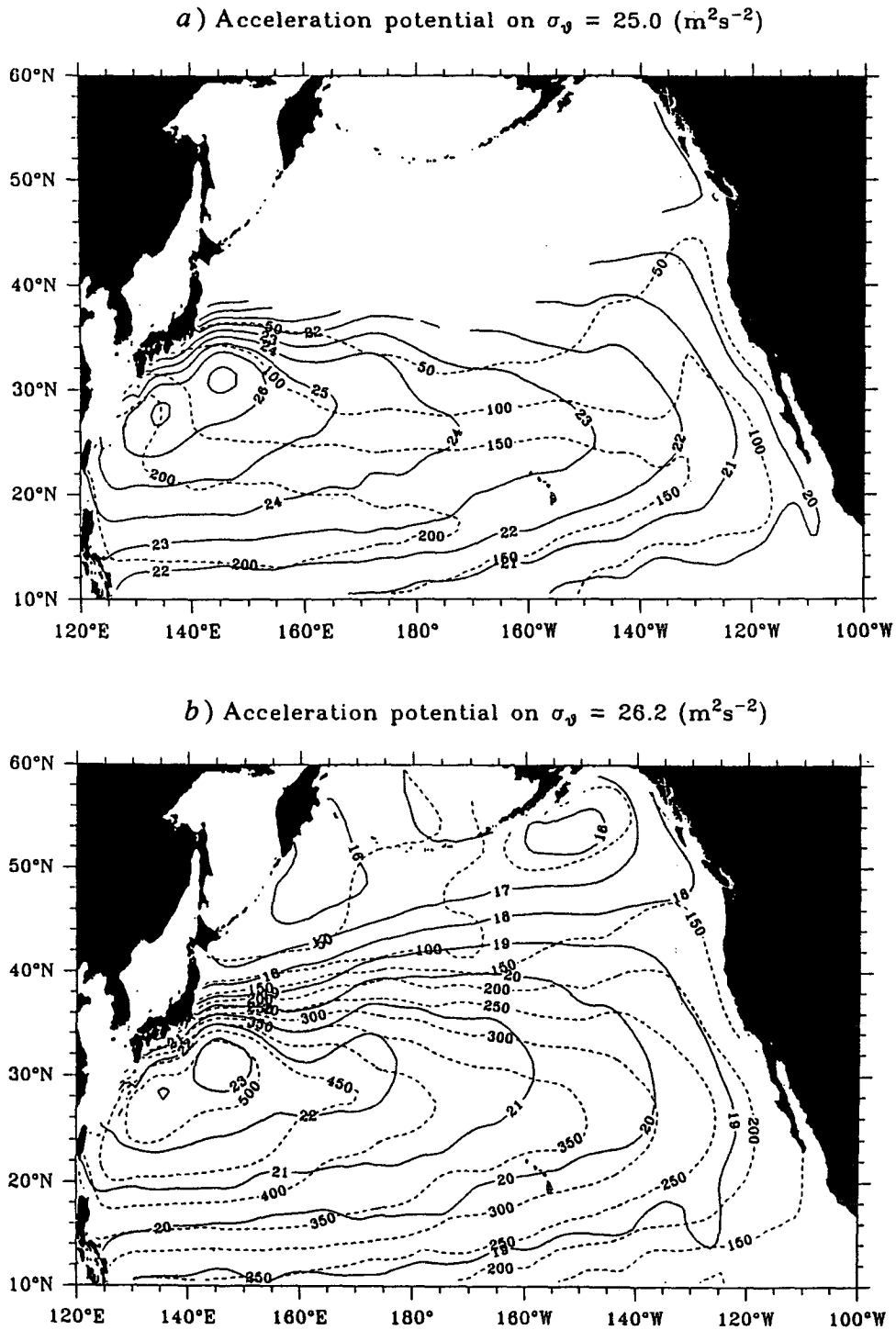


FIG. 3. Acceleration potential (solid lines, referenced to 2000 m) and depth contours (dashed lines) for isopycnal surface $\sigma_\theta = 25.0$ (a) and $\sigma_\theta = 26.2$ (b).

circulation, defined as the latitude that separates the eastward motion from the westward motion, migrates northward from shallow to deep isopycnal surfaces, that is, the northern intensification. For ex-

ample, the center of the gyre is at 26°N at $\sigma_\theta = 25$, but it moves to 31°N at $\sigma_\theta = 26.2$.

Assuming that the flow is geostrophic and diapycnal mixing is negligible, the acceleration potential isolines

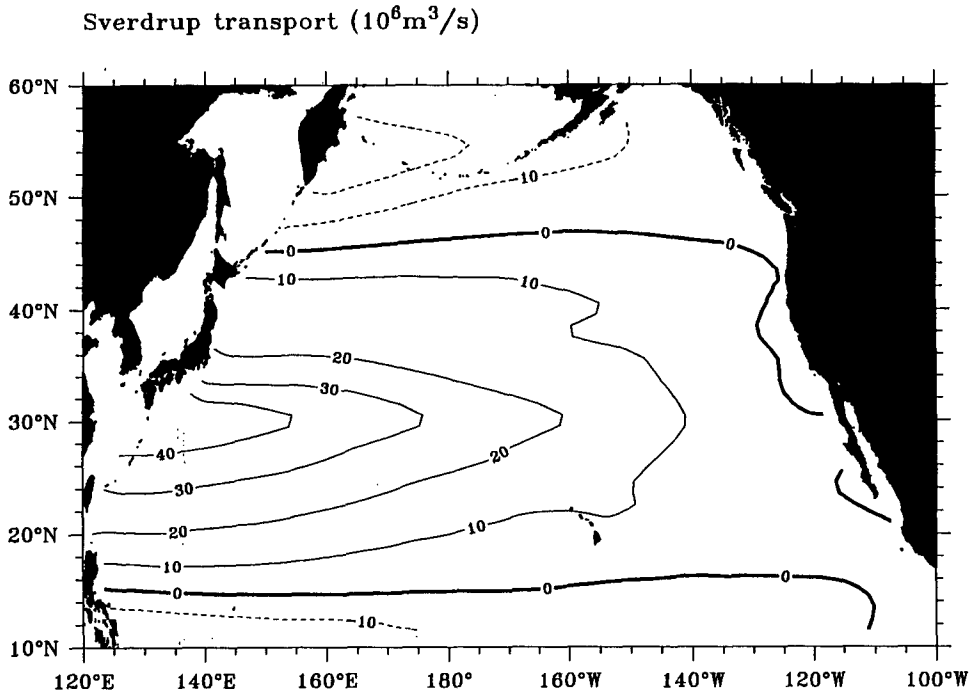


FIG. 4. Sverdrup transport streamfunction calculated using the (reduced by 20%) annual surface wind stress climatology by Hellerman and Rosenstein (1983).

can serve as streamlines, which indicate the water trajectories on each isopycnal surface. Within the northern and southern edges of the subtropical gyre, particle trajectories intersect the depth contours at small angles because the vertical velocity is small. Only in the middle of the subtropical gyre does the cross-isobath component become large due to strong Ekman pumping. Within the subpolar gyre particle trajectories actually go upward along isopycnals due to the positive Ekman velocity.

In the North Pacific, $\sigma_\theta = 26.2$ is the boundary between the ventilated thermocline and the unventilated thermocline. This isopycnal surface reaches a maximum depth of 500 m. Compared with the maximum depth of 800 m for the base of the ventilated thermocline ($\sigma_\theta = 27.1$) in the North Atlantic (Huang 1990), this is rather shallow. The shallowness of the ventilated thermocline in the North Pacific is associated with the strong stratification and the shallow mixed layer depth.

3) The annual-mean Ekman pumping velocity is calculated from the HR data. There has been concern about the drag coefficient used in the HR calculation. As Harrison (1989) and Trenberth et al. (1990) pointed out, the HR wind stress is about 20%–30% higher than the new results based on a more accurate bulk formula by Large and Pond (1981). For example, the maximum barotropic streamfunction in the subtropical North Pacific is about 62 Sv ($\text{Sv} \equiv 10^6 \text{ m}^3 \text{ s}^{-1}$) according to the HR data, but it is about 50 Sv according to the new wind stress data by Trenberth et al. (1990).

The momentum flux across the air–sea interface is a complicated function of the sea state and the atmospheric stability as discussed by Large and Pond (1981) and more recently by Huang et al. (1986). In this study our concern is the global structure of the wind-driven circulation, so the detailed structure of the wind stress is only of secondary importance. Thus, we have used the HR wind stress data reduced by a factor of 0.8, so that the maximum barotropic streamfunction is about 50 Sv, which is the same as the result by Trenberth et al. (1990). In addition, the factor of 0.8 is chosen to balance the total mass flux for the upper two kilometers of the North Pacific, as will be explained in detail in the next section. The barotropic streamfunction thus obtained is shown in Fig. 4.

Given the wind stress, the Ekman pumping velocity in spherical coordinates is calculated by the following equation:

$$w_{\text{Ek}} = \frac{1}{a\rho_0 2\Omega \sin\phi} \left(\frac{1}{\cos\phi} \frac{\partial\tau^\phi}{\partial\lambda} - \frac{\partial\tau^\lambda}{\partial\phi} + \frac{\tau^\lambda}{\sin\phi \cos\phi} \right). \quad (6)$$

The computed Ekman pumping velocity map is shown in Fig. 5a. For most of the subtropical gyre interior, the Ekman pumping rate is no larger than -50 m/yr , except along the southern rim of the gyre where the Ekman pumping rate can reach -75 m/yr .

From (3), the subduction rate consists of two terms, the vertical pumping at the base of the mixed layer

and the lateral induction due to the sloping of the mixed layer base. The vertical pumping is generally smaller than the Ekman pumping (Fig. 5b). However, the difference is small because the winter mixed layer in most parts of the subtropical North Pacific is no more than 100 m. In comparison, the winter mixed layer in the subtropical North Atlantic can reach more than 200 m.

The other contribution to the subduction is due to the lateral induction. Because the mixed layer base slopes, horizontal motion gives rise to water flows into the thermocline (Fig. 5c). Within the eastern basin, this contribution is smaller than that of the vertical pumping. For two small regions (near 130°W and 150°W), the lateral induction actually has a different sign, so it works against subduction due to vertical pumping. On the other hand, the lateral induction term reaches 100 m/yr near the center of the recirculation of the Kuroshio, which is due to the strong lateral gradient of winter mixed layer depth. Thus, the lateral induction dominates the subduction rate near the Kuroshio recirculation. However, along the southern rim of the subtropical gyre the mixed layer depth increases from 25 m in the eastern basin to 50 m in the western basin. As a result, the westward motion induces an entrainment from the main thermocline to the mixed layer, and this gives rise to a negative lateral induction along the southern rim of the subtropical gyre. This could give rise to entrainment into the mixed layer even if the local Ekman pumping is downward, as shown in the southern part of Fig. 5d. Marshall and Nurser (1991) also gave an example of water being entrained into the mixed layer in the southwestern part of a subtropical basin due to heating.

The sum of these two terms is the total subduction rate (Fig. 5d). The map of the subduction rate looks somewhat like the map of Ekman pumping rate, except it is moved slightly northward. In general, the subduction rate is larger than the Ekman pumping rate due to a combination of vertical pumping and lateral induction. The major difference is the strong subduction rate (about 100 m/yr) in the Kuroshio recirculation due primarily to the strong spatial gradient of mixed layer depth that gives rise to strong lateral induction.

3. Renewal rate of subtropical water masses and mass flux budget

Water masses in the subtropical oceans are renewed primarily through air–sea interaction. Although the connection between temperature/salinity and surface conditions in late winter has been recognized for a long time, a clear and quantitative dynamical picture of the subtropical water mass formation process emerged only recently through the systematic studies of ventilation (e.g., Stommel 1979; Woods 1985). The theoretical development of the three-dimensional structure of the wind-driven circulation, especially the exact definition of the subduction rate, gives a clear way of calculating the renewal time of these water masses.

In the subtropical gyre (defined as the region of negative wind stress curl), water mass volume distribution per each $0.2\sigma_\theta$ is calculated from the Levitus annual mean hydrography and shown in Fig. 6a. The domain in the following discussion is bounded on the east by the North American continent and the 110°W meridian, on the south by the 15°N meridian, on the west by the 135°E meridian, and on the north by a slanted line running from south of Japan to Vancouver Island along the (slightly smoothed) zero-wind-curl line. We have chosen the 135°E meridian, so that a clear picture of the mass balance is obtained without the complications of dealing with the western boundary current. The corresponding total ventilation rate is obtained by summing up the subduction rate within each strip of isopycnal outcropping area (Fig. 6b). The renewal time of each water mass is defined by the water mass volume divided by the ventilation rate (Fig. 6c).

The ventilation rate for isopycnals outcropping within the southern part of the subtropical gyre ($\sigma_\theta < 24.4$) is relatively small. However, the stratification in the upper part of the thermocline is strong, so the water mass volume is small. Consequently, the ventilation time for these water masses is short, about 5–6 years.

The ventilation rate for isopycnals outcropping in the middle of the subtropical gyre, density range of $\sigma_\theta = 24.4\text{--}25.2$, is large. In fact, the ventilation rate reaches a maximum of 4.6 Sv for the density range of $\sigma_\theta = 24.8\text{--}25.0$. Although the corresponding volume of this water mass is larger than that corresponding to the shallower isopycnals, the renewal time remains short (about 4.5 years).

There have been many studies devoted to the subtropical mode water in the North Pacific characterized by a thermostat around 16°C (e.g., Masuzawa 1969, 1972; McCartney 1982; Suga et al. 1989; Tally 1985). Although the subtropical mode water appears as a local maximum in the water mass volume distribution for the western North Pacific, it does not stand out as a local maximum in our statistics based on the Levitus data for the entire subtropical basin. The exact definition of the subtropical mode water in terms of the potential density varies from author to author because the water properties do change slightly along the trajectories. We choose the density range of $\sigma_\theta = 25.2\text{--}25.6$. According to our calculation, the ventilation rate of the subtropical mode water, corresponding to the density $\sigma_\theta = 25.2\text{--}25.4$, is 3.2 Sv. The volume of this water mass is about 948 000 km³, so the renewal time is about 9.4 years. For the density range of $\sigma_\theta = 25.4\text{--}25.6$ the ventilation rate is 2.0 Sv. The volume of this water mass is about 1 093 000 km³, so the renewal time is about 17.3 years.

Our estimated renewal time for the subtropical mode water is about 2–3 times longer than Worthington's estimation of 7 years for the North Atlantic subtropical mode water. Other estimations based on radioactive

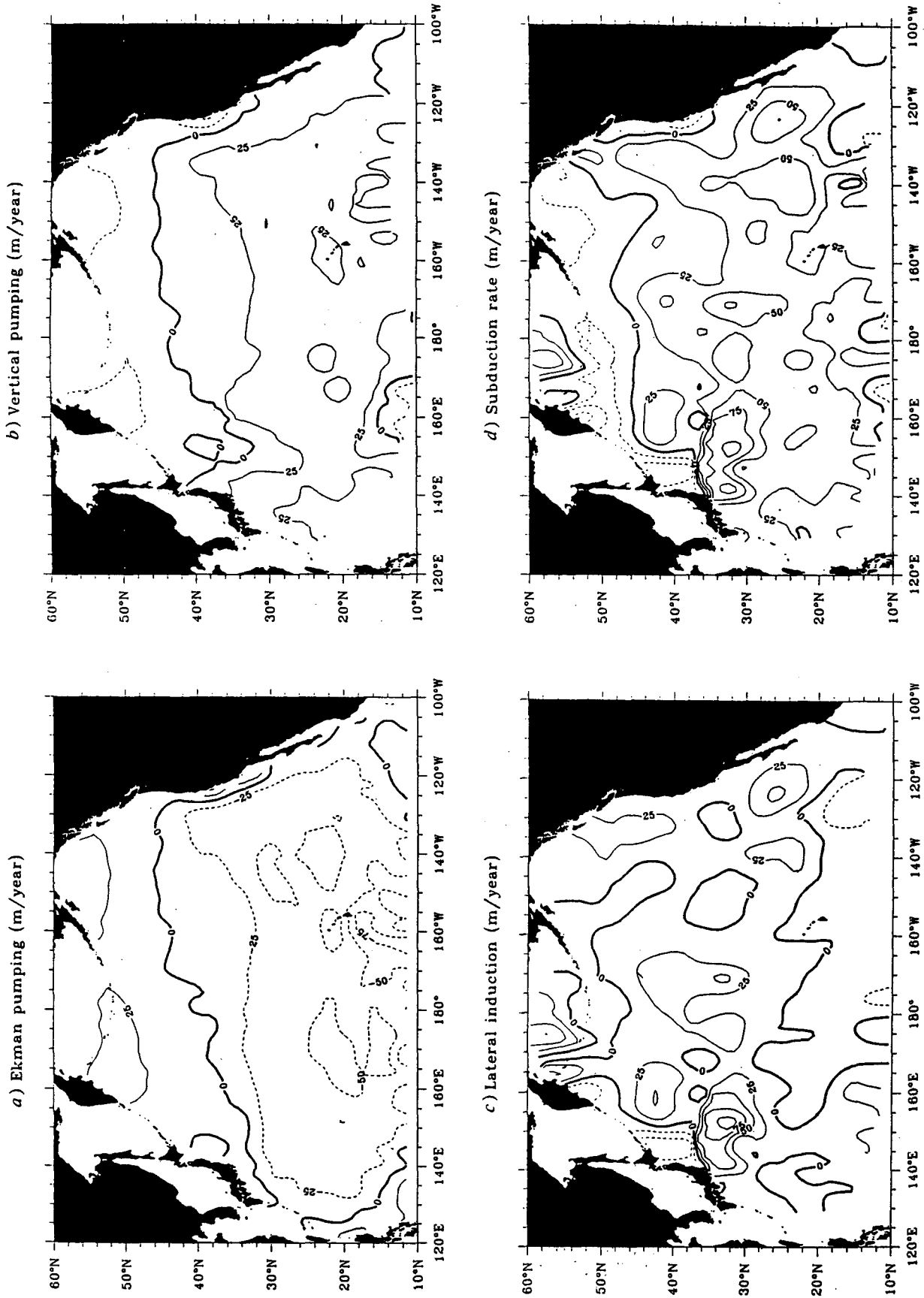


FIG. 5. (a) Ekman pumping rate; (b) vertical pumping rate at the base of the mixed layer; (c) lateral induction rate at the base of the mixed layer; (d) subduction rate.

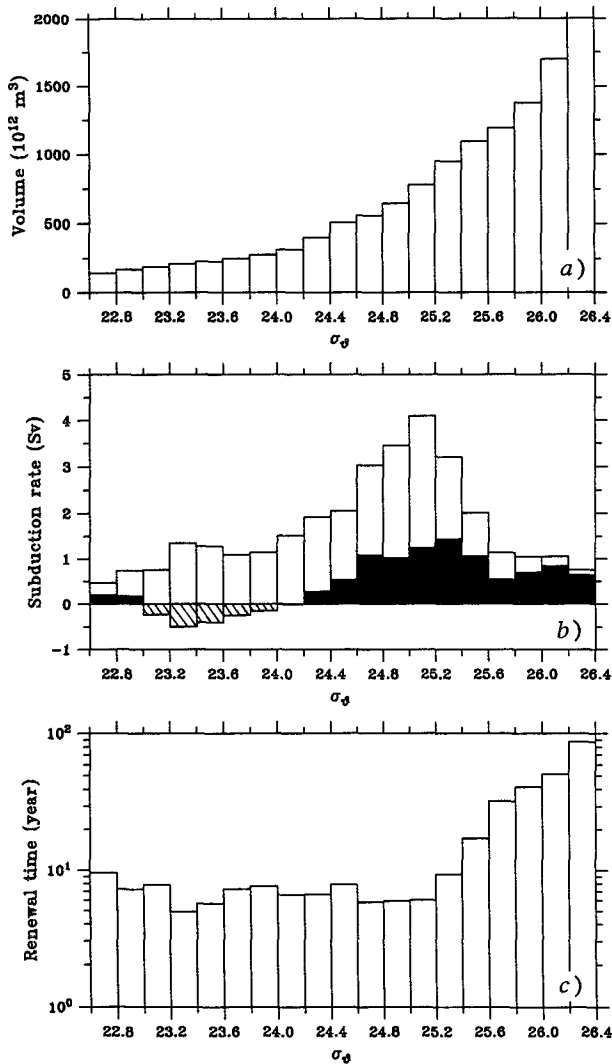


FIG. 6. (a) Water mass volume distribution in the North Pacific for each $0.2\sigma_\theta$ interval. (b) Ventilation rate for each $0.2\sigma_\theta$ interval. The dark column indicates the contribution due to lateral induction and the hollow column depicts the vertical pumping term. Notice that the shaded columns indicate negative contribution due to lateral induction, so the vertical pumping term is represented by the entire length of the column. (c) Water mass renewal time for $0.2\sigma_\theta$ interval.

tracers gave values of less than ten years for the North Atlantic subtropical mode water (Jenkins 1982; Sarmento 1983). Such a renewal time scale is consistent with the relatively stable properties of the subtropical mode water.

Notice that the renewal time of the subtropical mode water depends on the exact definition of the mode water. According to Masuzawa (1969, 1972) and Bingham (1992), the mode water that has a thermostad appears only west of the 180° meridian in the density range of $\sigma_\theta = 25.2\text{--}25.6$. Because the subduction rate is in general larger west of 180° , the renewal rate would

be shorter if we define the subtropical mode water to be where thermostad is found. In fact, we have carried out a calculation in which only properties west of 180° and north of 25°N are considered. As shown in Fig. 7, the renewal time for water in the density range of $\sigma_\theta = 25.2\text{--}25.4$ is reduced to 6.8 years (as opposed to 14.0 years shown in Fig. 6b); the renewal time remains almost the same for water in the density range of $\sigma_\theta = 25.4\text{--}25.6$.

In addition, the exact definition of the subtropical mode water can be slightly different. Suga et al. (1989) studied the water properties in the 137°E section and suggested that the subtropical mode water (defined as potential vorticity minimum) is found in the density range of $\sigma_\theta = 24.75\text{--}25.35$ in summer and $\sigma_\theta = 25.05\text{--}25.55$ in winter. Our analysis for the western basin (Fig.

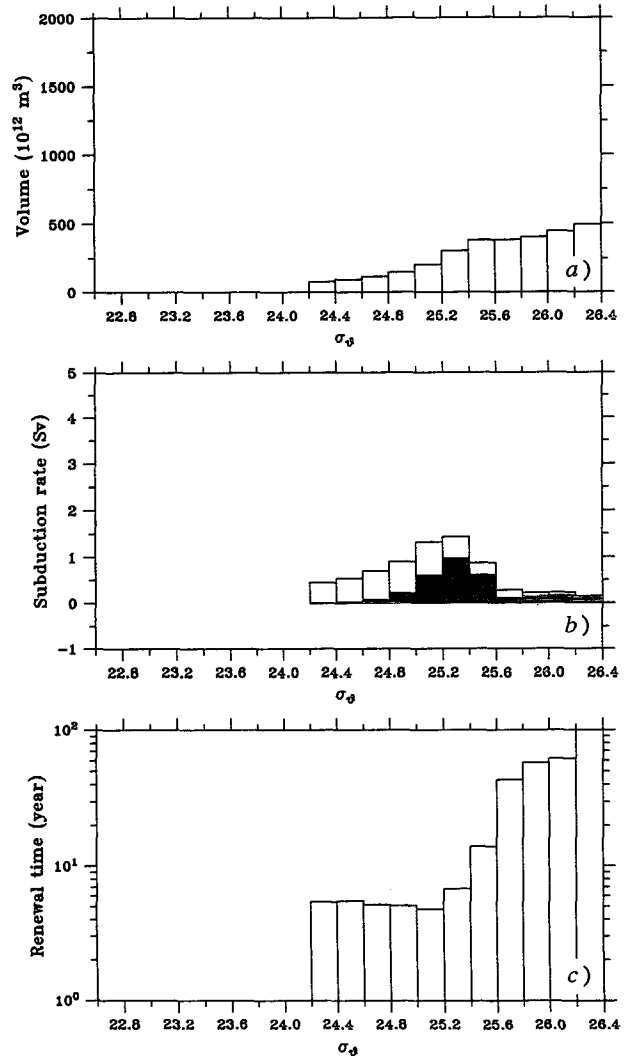


FIG. 7. Water mass volume distribution, ventilation rate, and renewal time for the western basin north of 25°N and west of 180° .

7b) does indicate a mode-water formation rate maximum within the density range of $\sigma_\theta = 24.8\text{--}25.2$.

For water masses denser than the mode water, the ventilation rate is substantially reduced because these isopycnals outcrop either in the northern part of the subtropical gyre where subduction is weak or has a different sign. Thus, these isopycnals are slowly ventilated (if ventilated at all), and the corresponding ventilation time is on the order of one century.

The mass flux partition for the subtropical North Pacific is shown in Fig. 8, where the wind-driven gyre is divided into four layers vertically, that is, the Ekman layer, the seasonal thermocline, the ventilated thermocline, and the unventilated thermocline. Notice that the Ekman layer is very thin (about 30 m), and the geostrophic mass flux within this depth is classified as part of the mass flux in the seasonal thermocline, so the Ekman layer is represented by just one thin sheet. Water is coming in from four sides in the form of Ekman flux. The northward Ekman flux across the southern boundary is large (21 Sv) because the Coriolis parameter is small at 15°N . The sum of these Ekman fluxes is equal to the total amount of Ekman pumping, 28.8 Sv.

Below the Ekman layer, the seasonal thermocline is defined as the water above the winter mixed layer base. Thus, the geostrophic mass flux includes the contribution from the upper 30 m of the ocean. The base of the seasonal thermocline is slightly slanted because the mixed layer depth reaches 175 m in the northwest corner, while it is 25 m in the southeast corner. The mass flux between the seasonal thermocline and the ventilated thermocline is about 33.1 Sv, of which the vertical pumping is 24.1 Sv and lateral induction only 9 Sv. By comparison, these two terms contribute about equally in the North Atlantic, that is, 12.1 Sv due to vertical pumping and 12.7 Sv due to lateral induction, according to Huang (1990). The reason for such a difference is due to the fact that the mixed layer in the North Pacific is relatively shallow and its bottom slope is small. Consequently, the vertical pumping term is very close to the Ekman pumping at the base of the Ekman layer. In addition, the lateral induction is small due to the small mixed layer depth gradient.

The vertically integrated mass flux budget for each layer is the following: Within the seasonal thermocline the total influx is 42 Sv and the efflux is 40.6 Sv, giving a net gain of 1.4 Sv. In the ventilated thermocline the total influx is 47.1 Sv and the efflux is 46.4 Sv, giving a net gain of 0.7 Sv. In the unventilated thermocline the total influx is 17.3 Sv and the efflux is 19.3 Sv, so there is a net loss of 2 Sv. The sum of the horizontal geostrophic fluxes in the seasonal thermocline, the ventilated thermocline, and the unventilated thermocline is 28.8 Sv, which is balanced by the Ekman pumping at the base of the Ekman layer. The small imbalances in the seasonal ventilated and unventilated thermoclines are possibly caused by the uncertainties

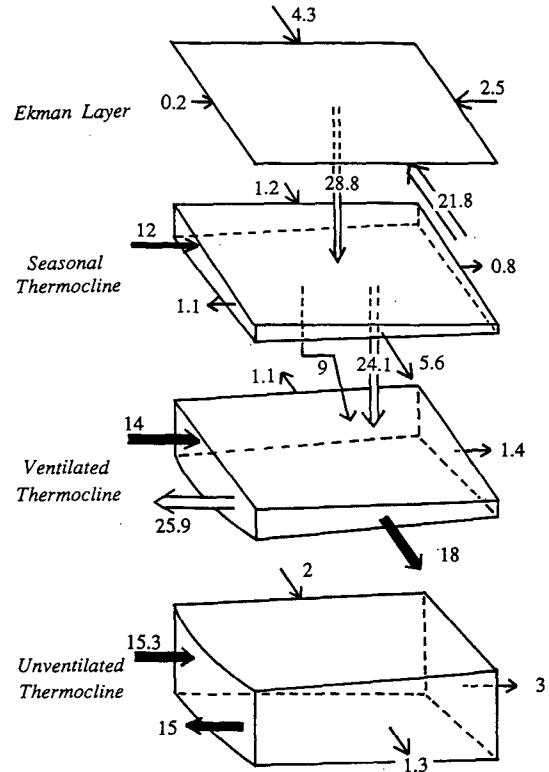


FIG. 8. Mass flux partition of the wind-driven circulation in the North Pacific, in Sv. The boundary between the seasonal thermocline and the ventilated thermocline is defined as the winter (March) mixed layer depth, and the base of the ventilated thermocline is defined as the $\sigma_\theta = 26.2$ isopycnal surface.

in estimating the geostrophic fluxes and by combining the HR wind data and Levitus climatology data, which have different estimation errors.

On the other hand, if the original HR data were used, without multiplication by a factor of 0.8, the total amount of Ekman pumping would be 36.0 Sv. Apparently, the geostrophic velocity below the Ekman layer, integrated from a reference level at 2000 m, can permit a horizontal divergence of only 28.8 Sv. Thus, the geostrophic velocity inferred from the Levitus data is unable to transport the extra mass flux of 7.2 Sv. This is the other reason for reducing the wind stress in the HR data. We repeated the same calculation using reference levels of 1500 m or 3000 m, but it has little influence upon the result presented in Fig. 8.

The unventilated thermocline is assumed to have no direct communication with the mixed layer, so there is no direct flux from above. The mass flux in the unventilated thermocline is calculated from geostrophic velocity relative to 2000 m for the depth between $\sigma_\theta = 26.2$ to the depth of 2000 m. According to the calculation, the total mass flux in the unventilated thermocline is 16.3 Sv, which consists of 35% of the total mass flux of the wind-driven circulation.

Another major difference between the North Pacific and the North Atlantic is the orientation of the zero-Ekman-pumping line, which is almost zonal in the North Pacific, but is northeastward in the North Atlantic. Since we have made use of an assumption of no baroclinic mode of water mass exchange across the zero-Ekman-pumping line, the meridional component of the geostrophic velocity is zero along the zero-Ekman-pumping line. As a result, water mass exchange across this line is due to the zonal velocity component. Thus, cross-gyre communication in our model is very small in the North Pacific because of the almost zonal orientation of the zero-Ekman-pumping line. In fact, the cross-gyre mass flux into the seasonal thermocline is only 1.2 Sv, and there is 1.1 Sv leaving the ventilated thermocline and 2.0 Sv coming into the unventilated thermocline. Therefore, the mass exchange across the intergyre boundary is quite small. In comparison, the intergyre mass exchange is large in the North Atlantic: it consists of 18.1 Sv for the seasonal thermocline, 11.0 Sv for the ventilated thermocline, and 6.5 Sv for the unventilated thermocline (Huang 1990).

Water mass conversion rates are very important parameters for oceanic circulation and climate study. Since water mass conversion is very closely related to air-sea interaction, there are many ways of estimating its rate. In the past, many studies have been devoted to the water mass conversion rate in the North Atlantic. Sarmiento (1983) used a tritium box model to study the thermocline and estimate the water mass formation rate. Speer and Tziperman (1992) used the air-sea heat flux and freshwater flux to estimate the water mass conversion rate. Although these studies gave rise to a slightly different estimate, they are not inconsistent with the results obtained by those using the recently developed theory of ventilation and subduction of the subtropical thermocline, such as Huang (1990), Marshall et al. (1993), Woods and Barkmann (1986), and Williams et al. (1994). We hope our results in this study will stimulate further study of the climatology of the North Pacific.

4. Conclusions

The structure of the wind-driven circulation in the subtropical North Pacific is diagnosed from the climatological data. Our calculation used the geostrophic velocity referenced to the 2000-m level plus the kinematic scheme for the subduction rate deduced from the Stommel demon. Thus, our calculation is based on the assumption that the effective subduction rate is very short, so that the subduction process can be accurately described by the Stommel demon. Based on analyzing the Levitus climatology, Marshall et al. (1993) have calculated the period of subduction over the North Atlantic. Although for the major part of the subtropical basin the estimated effective subduction period is relatively short (one to two months), it is

three to four months along the southern rim of the subtropical basin. Thus, the subduction rate based on the Stommel demon is questionable near the southern rim of the subtropical gyre. However, an exact estimation of the possible errors involved is rather complicated, and it is better to wait for results based on high quality datasets.

In this study, however, we have chosen not to calculate the subduction period because we believe that the Levitus dataset is not accurate enough for such a task. Although the dataset contains monthly mean temperatures, its salinity field is for the seasonal mean only; thus the mixed layer parameter diagnosed from the data is not accurate enough for describing the annual cycle of the mixed layer. The lack of monthly mean salinity data can be a major problem for calculating the mixed layer parameter in the North Pacific where the freshwater flux due to precipitation/evaporation plays an important role in setting up the mixed layer density. We hope to examine the annual cycle of the mixed layer and the subduction process in the near future using a dataset with higher time and spatial resolution.

Our calculation for the subtropical North Pacific provides a very interesting contrast between the North Pacific and the North Atlantic. The stratification in the North Pacific is stronger than that of the North Atlantic because surface water in the North Pacific is fresher. The strong stratification and freshness of the surface water gives rise to a relatively shallow mixed layer and gentle sloping of the mixed layer base in the North Pacific. As a result, the vertical pumping term (24.1 Sv) is very close to the Ekman pumping (28.8 Sv) and the lateral induction rate (9.0 Sv) is comparatively small. On the other hand, in the North Atlantic the vertical pumping (12.1 Sv) is noticeably smaller than the Ekman pumping (16.2 Sv), while the lateral induction (12.7 Sv) is large due to the strong north-south gradient of the mixed layer base. In fact, in the North Atlantic contributions to the subduction rate from the vertical pumping and lateral induction are comparable.

A major difference in the general circulation in these two oceans is the different modes of thermohaline circulation that exist. The North Atlantic is characterized by a strong meridional overturning cell driven primarily by cooling in the north and heating in the south. The North Pacific is characterized by a strong halocline (especially in the subpolar basin) and a very weak meridional overturning cell (if there is any) controlled primarily by the excess precipitation. Thus, the stratification, especially in the upper ocean, in the North Pacific is much stronger than that in the North Atlantic. The strong stratification in the upper ocean gives rise to a shallower mixed layer and a shallow thermocline in the North Pacific. The base of the ventilated thermocline reaches the maximum depth of 500 m. The zero-Ekman-pumping line is almost zonal in the North

Pacific, so the so-called intergyre communication term, which is an important term for the North Atlantic, is very small.

There is a major disadvantage of using the Levitus data because the dataset is averaged over several decades and highly smoothed in space and time. For example, the maximum mixed layer depth from our calculation may well underestimate that in the real ocean. Thus, the resulting mass flux partition may underestimate the flux in the ventilated thermocline. A more careful examination of the thermocline structure and its ventilation requires climatological data with higher quality.

Acknowledgments. R. X. Huang was supported through NOAA Grant NA36GP0270 and NSF Grant OCE93-00706. B. Qiu was supported by the Office of Naval Research under Grant N00014-92-J-1656.

APPENDIX

Subduction Rate Defined as an Integral Quantity

Subduction rate can be defined slightly differently, depending on the coordinates used. First, subduction rate can be defined in the Lagrangian sense (Woods 1985; Woods and Barkmann 1986). Accordingly, the annual mean subduction rate is

$$S_{\text{ann}}^L = -\frac{1}{T} \int_0^T w_{mb} dt - \frac{\Delta h_L}{T}, \quad (\text{A.1})$$

where T is the time of the average, taken as 1 year because of the seasonal cycle, the subscript mb indicates the base of the mixed layer, and Δh_L indicates the mixed layer depth change accumulated over one year's Lagrangian trajectory. Note that both terms include the temporal average over a year and the spatial average over the 1-year trajectory.

Second, an instant subduction rate in the Eulerian coordinates can be defined as (Cushman-Roisin 1987)

$$S = -\left(w_{mb} + \mathbf{u}_{mb} \cdot \nabla h + \frac{\partial h}{\partial t} \right). \quad (\text{A.2})$$

Since the instantaneous subduction rate fluctuates so much, it is more meaningful to use the annual mean subduction rate defined as

$$S_{\text{ann}}^E = \frac{1}{T} \int_{T_s}^{T_e} S dt, \quad (\text{A.3})$$

where T_s and T_e are the time when the effective subduction started and ended, and S_u is the instantaneous subduction rate defined in (A.2). A pitfall in calculating the annual mean subduction rate is using a simple Eulerian mean over the whole year:

$$\overline{S_{\text{ann}}^E} = \frac{1}{T} \int_0^T S dt. \quad (\text{A.4})$$

Substituting (A.2), this would lead to a wrong estimation of $\overline{S_{\text{ann}}^E} = -\overline{w_{mb}} - \overline{\mathbf{u}_{mb} \cdot \nabla h}$. In general, this tends to underestimate the annual mean subduction rate.

To compare these different definitions of subduction rates, we will discuss a simple meridional section on a β plane (Cushman-Roisin 1987):

$$f = f_{00} + \beta(\phi - 45), \quad (\text{A.5})$$

where $f_{00} = 3200 \text{ yr}^{-1}$, $\beta = 67 \text{ yr}^{-1} \text{ deg}^{-1}$, and ϕ is the latitude, in degrees. We will assume the vertical velocity is only a linear function of ϕ :

$$\frac{d\phi}{dt} = v = \phi - 45. \quad (\text{A.6})$$

The Ekman pumping velocity is

$$w_e = 4.2(\phi - 45), \quad (\text{A.7})$$

where w_e is in meters per year. We will further assume that mixed layer density is only a function of latitude, so there is no vertical shear in the meridional velocity. Neglecting the relative vorticity, the vorticity equation is $\beta v = f w_z$. The trajectories of water particles can be integrated in closed form.

The mixed layer is assumed to be deep in the north and shallow in the south, and it varies with the season:

$$h(\phi, t) = 20 + 60 \left(1 + \frac{\phi - 45}{16} \right) (1 - g(t)), \quad (\text{A.8})$$

where $g(t)$ varies from 0 at late winter to 1 at later summer. For comparison, two profiles are used. The first profile is a simple sinusoidal profile,

$$g_1(t) = \frac{1 - \cos(2\pi t)}{2}, \quad 0 \leq t \leq 1,$$

while the second profile $g_2(t)$, shown in Fig. A1, fits the mixed layer profile calculated by Woods (1985).

As an example, we choose a station at $\phi_0 = 41.5$. In calculating the subduction rate, it is important to monitor the fate of the subducted water. One has to follow the trajectories of water leaving the mixed layer. First, the subduction does not begin exactly at $t = 0$; instead, it starts at $T_s = -0.0244$ [using profile $g_1(t)$]. The second step is catching the moment when the effective subduction stops, which is marked by the last trajectory that barely escapes the mixed layer entrainment downstream. The time T_e when this trajectory is started marks the end of the effective subduction, so the Eulerian subduction rate can be calculated from (A.3). The subduction rate in the Lagrangian sense can be calculated by following this last trajectory, as shown in Fig. A2.

The major difference between these two definitions of subduction rate is the following. In Eulerian coordinates, water parcels are released from the base of the mixed layer at a fixed location; the trajectories of these

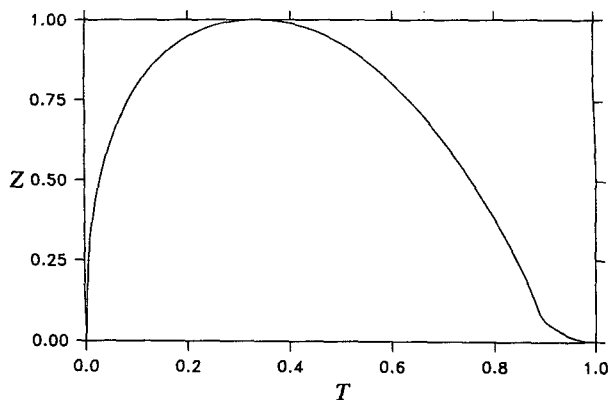


FIG. A1. The mixed layer depth as a function of time, $g_2(t)$.

parcels are to be tracked (Cushman-Roisin 1987). In Lagrangian coordinates, water parcels are released from the base of the mixed layer at a location determined by the trajectory of the original parcel, and these trajectories are to be tracked (Woods and Barkmann 1986).

Calculating the annual mean subduction rate according to these two definitions requires accurate information of the spatial and temporal evolution of the mixed layer. However, such detailed information is almost impossible to obtain from any climatological data. Thus, we propose a simple way of calculating the subduction rate, simply by

$$S_{ann} = (d_2 - d_1) + (h_{m,1} - h_{m,2}), \quad (A.9)$$

where d and h are the depth of the trajectory and the mixed layer base, and subscripts 1 and 2 indicate the

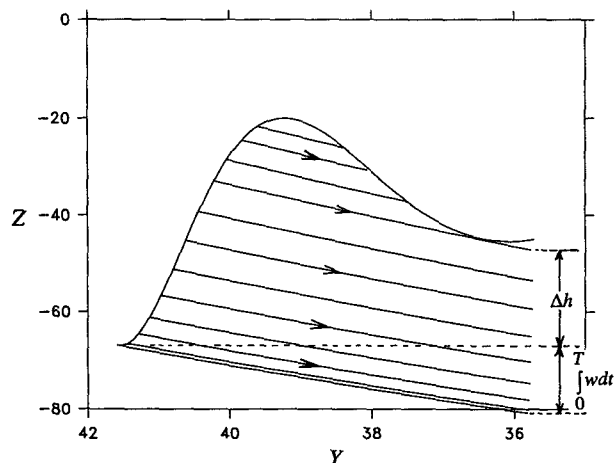


FIG. A2. Subduction and recapture of water parcels in a Lagrangian model, depth in meters, meridional coordinate in degrees. The top curve indicates the base of the mixed layer in the moving coordinates, while the long sloping lines indicate the trajectories of water parcels released from the base of the mixed layer.

TABLE A1. Subduction rate calculated by different definitions, in $m\ yr^{-1}$.

Profile	S_{ann}^L	S_{ann}^E	S_{ann}	T_s	T_e
$g_1(t)$	33.73	30.17	36.93	-0.0244	0.2563
$g_2(t)$	33.21	35.00	36.93	-0.0403	0.0727

first and the second winter. For the simple profiles $g_1(t)$ and $g_2(t)$, the corresponding subduction rates are listed in Table A1.

Although subduction rates calculated according to these definitions are slightly different for the first case with $g_1(t)$, the differences for the second case with $g_2(t)$ are rather small. This is due to the fast mixed layer detrainment in spring, which gives rise to a very short duration of the effective subduction. As a result, subduction rates calculated according to different definitions are very close. Note that the differences between these definitions are much smaller than other possible errors generated during calculating the subduction rate from the climatological data. The temporal resolution of the Levitus data is very crude. In fact, although temperature is compiled for each month, the salinity data are compiled for the seasons only. It is very difficult to calculate the time evolution of the mixed layer depth. Therefore, our definition (A.9) can serve as a convenient and practical tool of calculating the subduction rate from climatological data with errors comparable with other processes.

REFERENCES

Bingham, F. M., 1992: Formation and spreading of subtropical mode water in the North Pacific. *J. Geophys. Res.*, **97**, 11 177-11 189.

Cushman-Roisin, B., 1987: Subduction. *Dynamics of the Oceanic Surface Mixed Layer, Proc. Hawaiian Winter Workshop*, Honolulu, Univ. of Hawaii at Manoa, 181-196.

Harrison, D. E., 1989: On climatological mean wind stress and wind stress curl fields over the world ocean. *J. Phys. Oceanogr.*, **19**, 57-70.

Hellerman, S., and M. Rosenstein, 1983: Normal monthly wind stress over the world ocean with error estimates. *J. Phys. Oceanogr.*, **13**, 1093-1104.

Huang, N. E., L. F. Bliven, S. R. Long, and P. S. DeLeonibus, 1986: A study of the relationship among wind speed, sea state, and the drag coefficient for a developing wave field. *J. Geophys. Res.*, **91**, 7733-7742.

Huang, R. X., 1990: On the three-dimensional structure of the wind-driven circulation in the North Atlantic. *Dyn. Atmos. Oceans*, **15**, 117-159.

—, 1991: The three-dimensional structure of wind-driven gyres: Ventilation and subduction. U.S. Natl. Report to Int. Union Geod. Geophys. 1987-1990. *Rev. Geophys. (Suppl.)*, 590-609.

Iselin, C. O'D., 1939: The influence of vertical and lateral turbulence on the characteristics of the waters at mid-depths. *Trans. Am. Geophys. Union*, **20**, 414-417.

Jenkins, W. J., 1982: On the climate of a subtropical ocean gyre: Decade time-scale variations in water mass renewal in the Sargasso Sea. *J. Mar. Res.*, **40**, 265-290.

—, 1987: 3H and He in the beta triangle: Observations of gyre ventilation and oxygen utilization rates. *J. Phys. Oceanogr.*, **17**, 763-783.

- Large, W. G., and S. Pond, 1981: Open ocean momentum flux measurements in moderate to strong winds. *J. Phys. Oceanogr.*, **11**, 324–336.
- Levitus, S., 1982: *Climatological Atlas of the World Ocean*. NOAA Prof. Paper No. 13, U.S. Dept. of Commerce, Washington, D.C., 173 pp.
- Luyten, J. R., J. Pedlosky, and H. Stommel, 1983: The ventilated thermocline. *J. Phys. Oceanogr.*, **13**, 292–309.
- Marshall, J. C., and A. J. G. Nurser, 1991: A continuously stratified thermocline model incorporating a mixed layer of variable thickness and density. *J. Phys. Oceanogr.*, **21**, 1780–1792.
- , —, and R. G. Williams, 1993: Inferring the subduction rate and period over the North Atlantic. *J. Phys. Oceanogr.*, **23**, 1315–1329.
- Masuzawa, J., 1969: Subtropic mode water. *Deep-Sea Res.*, **16**, 463–472.
- , 1972: Water characteristics of the North Pacific central region. *Kuroshio, Its Physical Aspects*, H. Stommel and K. Yoshida, Eds., University of Washington Press, 95–128.
- McCartney, M. S., 1982: The subtropical recirculation of mode waters. *J. Mar. Res.*, **40**(Suppl.), 427–464.
- Montgomery, R. B., and E. D. Stroup, 1962: Equatorial waters and currents at 150°W in July–August 1952. *Johns Hopkins Oceanogr. Studies*, No. 1, 68 pp.
- Needler, G. T., 1971: Thermocline models with arbitrary barotropic flow. *Deep-Sea Res.*, **18**, 895–903.
- Rhines, P. B., and W. R. Young, 1982a: Homogenization of potential vorticity in planetary gyres. *J. Fluid Mech.*, **122**, 347–367.
- , and —, 1982b: A theory of the wind-driven circulation. I. Mid-ocean gyres. *J. Mar. Res.*, **40**(Suppl.), 559–596.
- Roemmich, D., and T. McCallister, 1989: Large scale circulation of the North Pacific Ocean. *Progress in Oceanography*, Vol. 22, Pergamon Press, 171–204.
- Sarmiento, J. L., 1983: A tritium box model of the North Atlantic thermocline. *J. Phys. Oceanogr.*, **13**, 1269–1274.
- Speer, K., and E. Tziperman, 1992: Rates of water mass formation in the North Atlantic Ocean. *J. Phys. Oceanogr.*, **22**, 93–104.
- Stommel, H. M., 1979: Determination of water mass properties of water pumped down from the Ekman layer to the geostrophic flow below. *Proc. Natl. Acad. Sci. USA*, **76**, 3051–3055.
- Suga, T., K. Hanawa, and Y. Toba, 1989: Subtropical mode water on the 137°E section. *J. Phys. Oceanogr.*, **19**, 1605–1618.
- Talley, L. D., 1985: Ventilation of the subtropical North Pacific: The shallow salinity minimum. *J. Phys. Oceanogr.*, **15**, 633–649.
- Trenberth, K. E., W. G. Large, and J. G. Olson, 1990: The mean annual cycle in global ocean wind stress. *J. Phys. Oceanogr.*, **20**, 1742–1760.
- Tsuchiya, M., 1982: On the Pacific upper-water circulation. *J. Mar. Res.*, **40**(Suppl.), 777–799.
- Welander, P., 1959: An advective model of the ocean thermocline. *Tellus*, **3**, 309–318.
- Williams, R. G., M. A. Spall, and J. C. Marshall, 1994: Does Stommel's mixed layer demon work? *J. Phys. Oceanogr.*, **24**, submitted.
- Woods, J. D., 1985: The physics of thermocline ventilation. *Coupled Ocean-Atmosphere Models*, Chapter 34. J. C. J. Nihoul, Ed., Elsevier, Amsterdam, 543–590.
- , and W. Barkmann, 1986: A Lagrangian mixed layer model of Atlantic 18°C water formation. *Nature*, **319**, 574–576.